Supporting Information for

Ligand Coordination Controlled by Monomer Binding: a Hint from DFT for Stereoselective Lactide Polymerization

Massimo Christian D'Alterio,[1] Serena Moccia,[1] Yolanda Rusconi,[2] Claudio De Rosa,[1] Giovanni Talarico*[1,2]

[1] Department of Chemical Sciences, Università degli Studi di Napoli Federico II, via Cintia, 80126 Napoli, Italy

[2] Scuola Superiore Meridionale, Largo San Marcellino 10, I-80138 Napoli, Italy

Table of Contents

Computational Details

All the density functional theory (DFT) calculations were performed using the Gaussian09 package.[S1] Geometry optimizations were performed using the B3LYP functional of Becke[S2] and the standard split-valence basis set with a polarization function of Ahlrichs and coworkers (SVP keyword in Gaussian)[S3] for H, N, O and C atoms whereas 6-311G(d,p)[S4] was employed at the Al center to achieve a better description of the coordination geometry. Geometry optimizations were performed without symmetry constraints. Transition states (TSs) were approached through a linear transit procedure using the forming or disappearing C–O bond as the reaction coordinate. All the geometries discussed in this work were confirmed as minima or TSs by frequency calculations. Finally, single-point energy calculations in solution were performed with the triple-ζ basis set 6-311G(d,p)[4] for H, N, O, C and Al. Solvent effects were included with the polarizable continuous solvation model PCM using toluene solvent.[S5] The influence of the dispersion correction was considered with the model GD3BJ (B3LYP-D3BJ).[S6] The Gibbs' free energy value associated to each structure was calculated considering the contribute of thermal and electronic energies with the related correction obtained by the SP energy calculation. This computational approach has been validated by considering the ratio between the experimental kinetic constants for the reported systems[S7,S8] and by using the Boltzmann distribution equation (Table S4).

The $\%V_{Bur}$ reported in the paper have been computed using the Samb*V*ca package.[S9] The program analyzes the first coordination sphere around the metal, which is the place where catalysis occurs. The optimized geometry of the TSs complexes under analysis has been properly oriented. After this alignment step the metal, the monomer and the growing chain have been removed, and the first coordination sphere (with radius $R = 4.0$ Å) around the metal is analyzed.

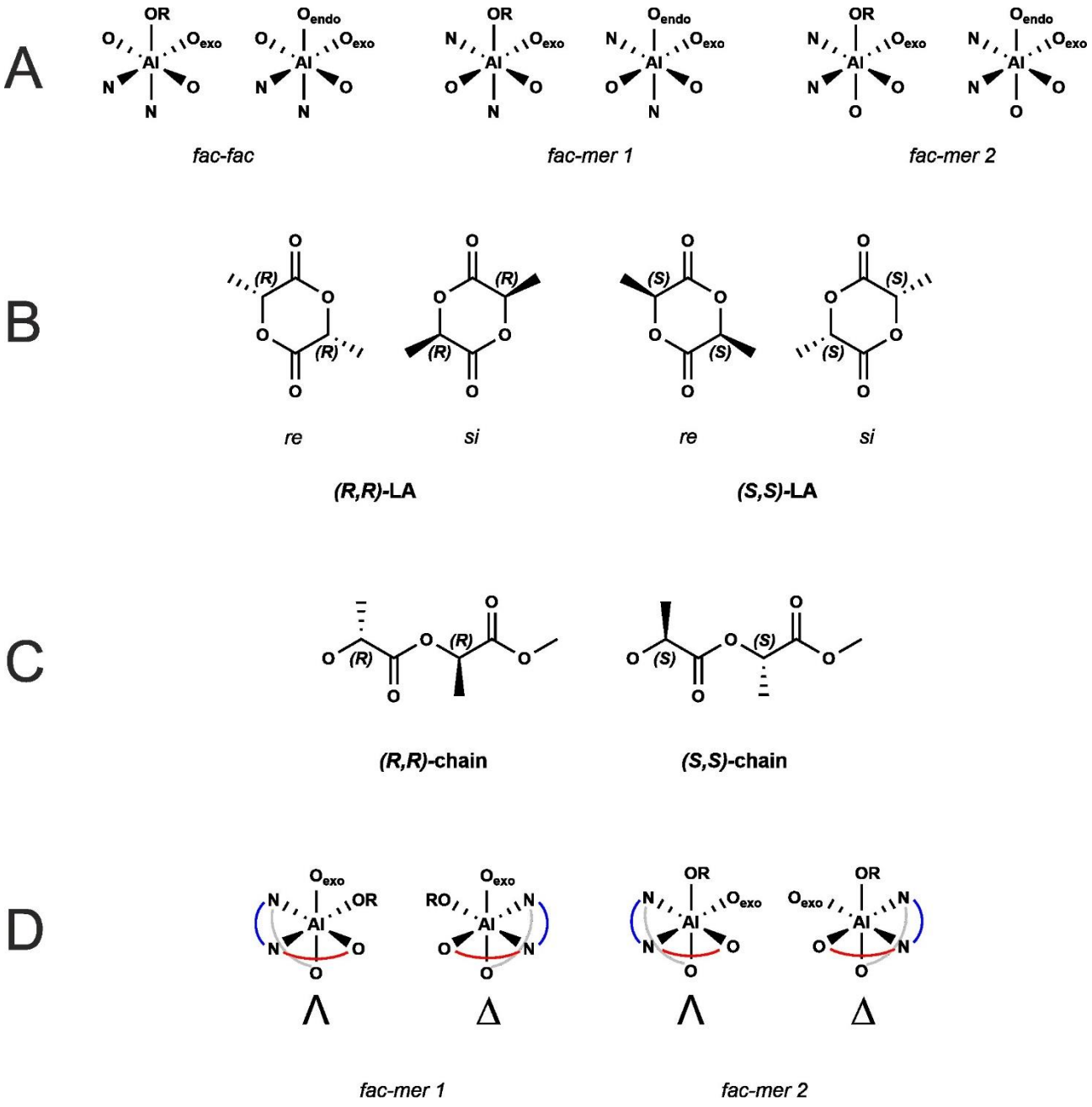

Scheme S1. List of elements of chirality considered in this work. With OR we called the OMe and with O_{endo} and/or O_{exo} we defined the endocyclic and exocyclic O of lactide (A); monomer chiralities (*RR*-LA and *SS*-LA) as well as the monomer enantiofaces (*re* and *si*) (B); chirality of the growing chain (*RR*-chain and *SS*-chain) (C); octahedral configuration for *fac-mer* 1 and *fac-mer* 2 wrapping mode during the ROP (D).

Table S1. TSs Gibbs energies (Δ*G*, in kcal/mol, with respect to *SS*-LA + INT2-*fm*2) for the reaction paths computed for *SS*-LA propagation promoted by system (*R*)-**1**. Values calculated in toluene. In bold red the low-lying paths

Chain Monomer Enantioface	*SS* *SS* *re*				Chain Monomer Enantioface	*SS* *SS* *si*			
		TS1		**TS2**			**TS1**		**TS2**
	A	20.3		18.5		A	17.3		21.9
Mechanism 1 (**M1**)	B	20.4		15.3	Mechanism 1 (**M1**)	B	18.9		19.1
	C	**16.2**		12.1		C	18.4		17.7
		TS1		**TS2**			**TS1**		**TS2**
Mechanism 2 (**M2**)	A	20.3		15.3	Mechanism 2 (**M2**)	A	17.3		19.1
	B	20.4		18.5		B	18.9		21.9
		TS1	**TSα**	**TS2**			**TS1**	**TSα**	**TS2**
	A	16.2	17.3	18.5		A	18.4	16.4	21.9
Mechanism 3 (**M3**)	B	16.2	17.3	15.3	Mechanism 3 (**M3**)	B	18.4	16.4	19.1
	C	20.3	17.3	12.1		C	17.3	16.4	17.7
	D	20.4	17.3	12.1		D	18.9	16.4	17.7

Table S2. TSs Gibbs energies (Δ*G*, in kcal/mol, with respect to *SS*-LA + INT2-*fm*2) for the reaction paths computed for *SS*-LA propagation promoted by system (*R*,*R*)-**2A**. Values calculated in toluene. In bold red the low-lying paths.

Chain Monomer Enantioface	*SS* *SS* *re*			Chain Monomer Enantioface	*SS* *SS* *si*		
		TS1	**TS2**			**TS1**	**TS2**
Mechanism 1 (**M1**)	A	18.8	13.3	Mechanism 1 (**M1**)	A	15.8	20.8
	B	**11.3**	**10.6**		B	12.9	16.8
		TS1	**TS2**			**TS1**	**TS2**
Mechanism 2 (**M2**)	A	18.8	10.6	Mechanism 2 (**M2**)	A	15.8	16.8
	B	11.3	13.3		B	12.9	20.8

Table S3. TSs Gibbs energies (Δ*G*, in kcal/mol, with respect to *RR*-LA + INT2-*fm*1) for all reaction paths computed for *RR*-LA propagation promoted by system (*R*,*R*)-**2A**. Values calculated in toluene. In bold red the low-lying paths.

Chain Monomer Enantioface	*RR* *RR* *re*			Chain Monomer Enantioface	*RR* *RR* *si*		
		TS1	**TS2**			**TS1**	**TS2**
Mechanism 1 (**M1**)	A	14.5	12.5	Mechanism 1 (**M1**)	A	15.1	10.0
	B	13.5	14.9		B	20.4	15.3
		TS1	**TS2**			**TS1**	**TS2**
Mechanism 2 (**M2**)	A	14.5	14.9	Mechanism 2 (**M2**)	A	15.1	15.3
	B	**13.5**	**12.5**		B	20.4	10.0

Table S4. Comparison of the calculated ΔΔ*G* considering various reaction paths based on: a fixed ligand wrapping mode (*fac-mer*, first column); different wrapping mode for D and L-LA (second column); our model proposed in the main text (third column) and the experimental $\Delta\Delta G_{exp}$ for *rac*-LA ROP promoted by systems (*R*)-**1** and (*R*,*R*)-**2A**.

System	$\Delta\Delta G_{calc}$[a]	$\Delta\Delta G_{calc}$[b]	$\Delta\Delta G_{calc}$[c]	$\Delta\Delta G_{exp}$[d]
(*R*)-**1**	4.0	-0.2	1.8	2.0
(*R*,*R*)-**2A**	\	3.6	2.2	2.3

[a]Calculated considering only *fac-mer* wrapping mode [b]Calculated considering only Mechanism 1 [c]Calculated with our model [d]Experimental value calculated using the ratios $k_{RR}/k_{SS} = 20$ for (*R*)-**1**) and $k_{SS}/k_{RR} = 25$ for (*R*,*R*)-**2A** within Arrhenius equation.

Table S5. TSs Gibbs energies (Δ*G*, in kcal/mol, with respect to *SS*-LA + INT2-*fm*1) for all reaction paths computed for *SS*-LA insertion into the Al-*RR*-chain bond for system (*R*,*R*)-**2A**. Values calculated in toluene. In bold red the low-lying paths.

Chain Monomer Enantioface	*RR* *SS* *re*			Chain Monomer Enantioface	*RR* *SS* *si*		
		TS1	**TS2**			**TS1**	**TS2**
Mechanism 1 (**M1**)	A	17.4	10.5	Mechanism 1 (**M1**)	A	14.0	19.4
	B	**14.5**	**10.3**		B	16.7	18.4
		TS1	**TS2**			**TS1**	**TS2**
Mechanism 2 (**M2**)	A	17.4	10.3	Mechanism 2 (**M2**)	A	14.0	18.4
	B	14.5	10.5		B	16.7	19.4

Table S6. TSs Gibbs energies (Δ*G*, in kcal/mol, with respect to *RR*-LA + INT2-*fm*2) for all reaction paths computed for *RR*-LA insertion into the Al-*SS*-chain bond for system (*R*,*R*)-**2A**. Values calculated in toluene. In bold red the low-lying paths.

Chain Monomer Enantioface	*SS* *RR* *re*			Chain Monomer Enantioface	*SS* *RR* *si*		
		TS1	**TS2**			**TS1**	**TS2**
Mechanism 1 (**M1**)	A	16.0	16.6	Mechanism 1 (**M1**)	A	**13.9**	**10.7**
	B	12.0	15.6		B	14.6	13.7
		TS1	**TS2**			**TS1**	**TS2**
Mechanism 2 (**M2**)	A	16.0	15.6	Mechanism 2 (**M2**)	A	13.9	13.7
	B	12.0	16.6		B	14.6	10.7

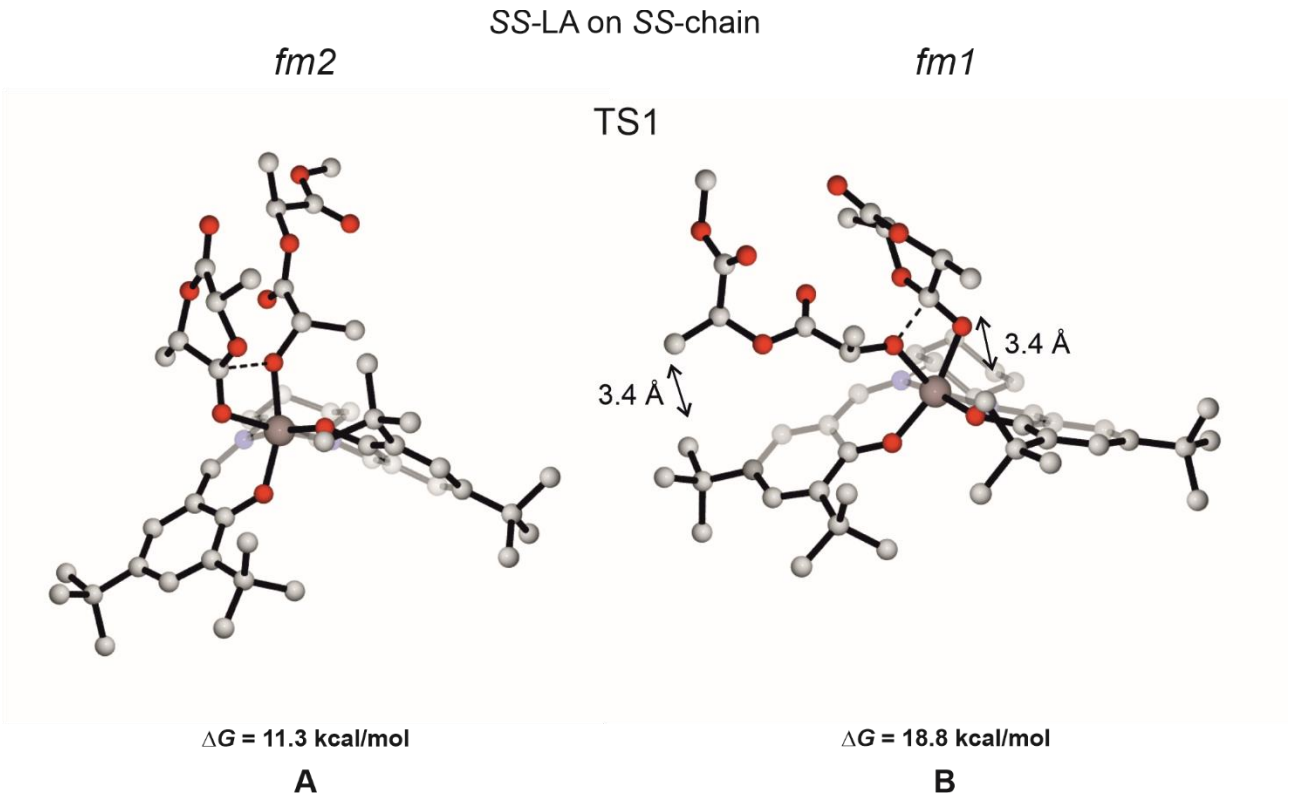

Figure S1. Optimized DFT geometries for the RLS of *SS* chain + *SS*-LA polymerization promoted by (*R*,*R*)-**2A** corresponding to the nucleophilic addition (TS1). The energetic preference of *fm*2 wrapping mode (A) with respect to *fm*1 (B) is due to lower steric interactions reported with arrows.

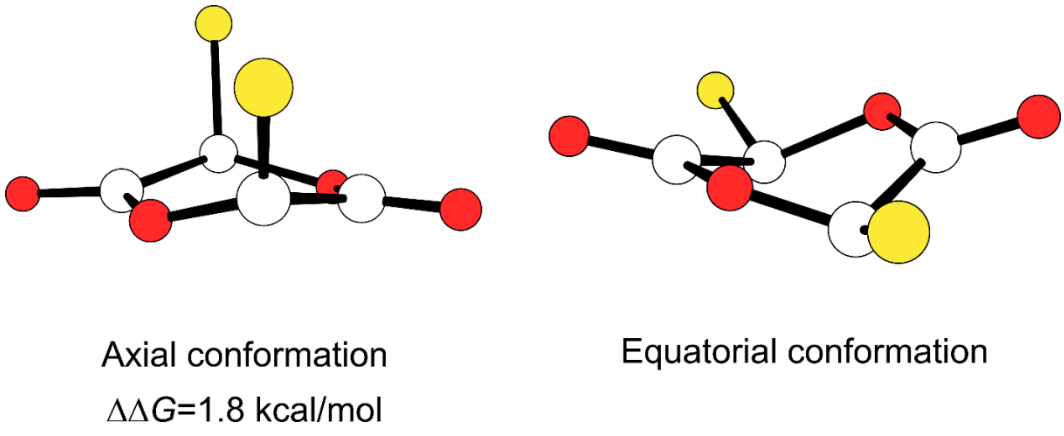

Figure S2. Structures of the two possible conformations adopted by LA monomers (in figure, the *R*,*R*) as isolated molecule. Axial conformation is more stable of 1.8 kcal/mol. In red, the oxygen atoms, in white the carbon atoms and in yellow are highlighted the carbon constituting the methyl moieties.

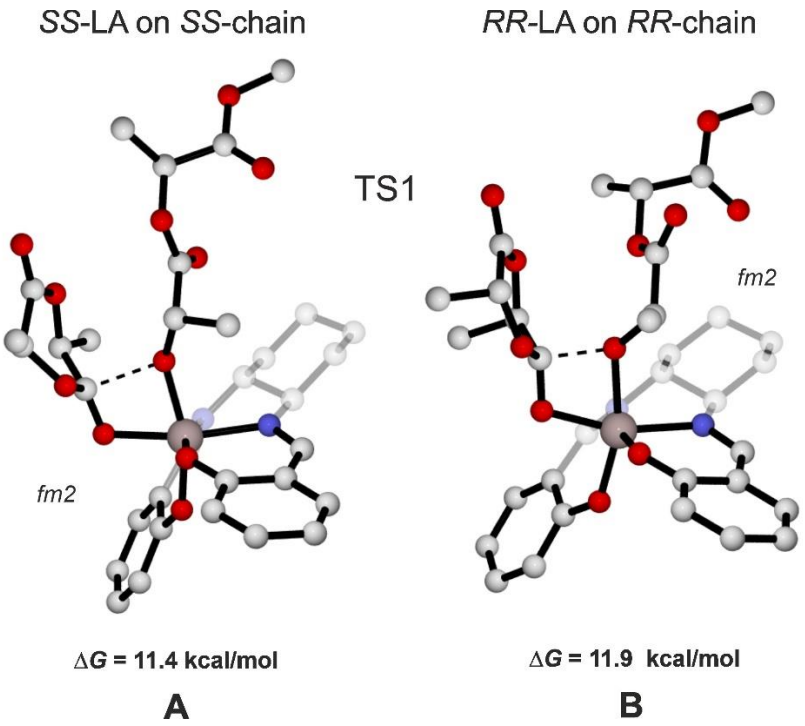

Figure S3. Optimized DFT geometries for the RLS of *SS* chain + *SS*-LA polymerization (*fm*2 wrapping mode) *vs*. *RR* chain + *RR*-LA polymerization (*fm*2 wrapping mode) promoted by (*R*,*R*)-**2B.** Both correspond to the nucleophilic addition (TS1).

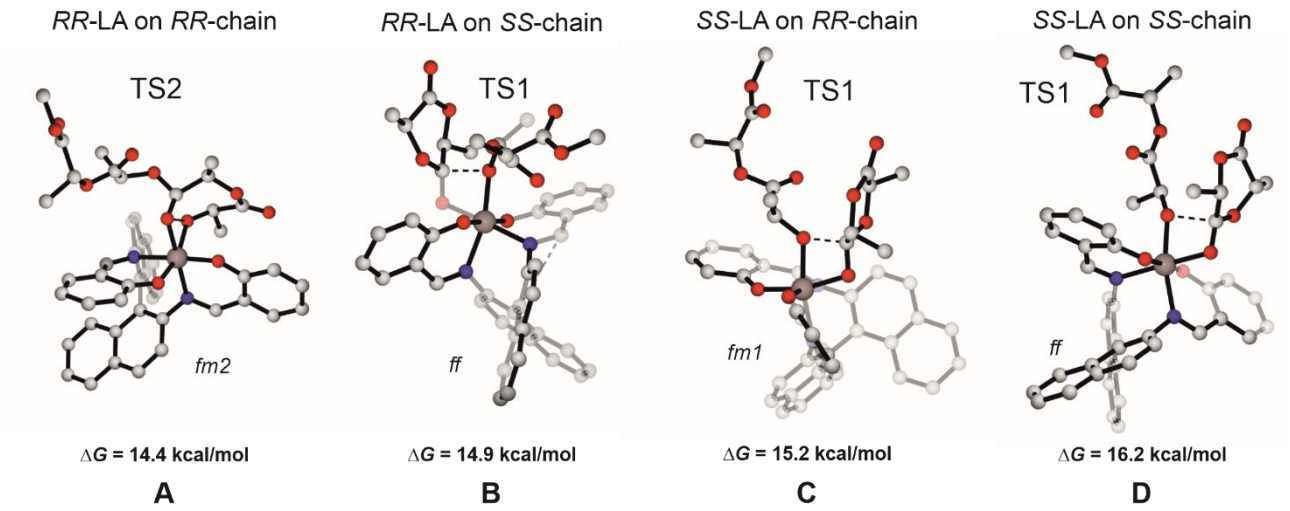

Figure S4. TSs geometries for the RLS of the (*R*)-**1** of (A) isotactic and (B) heterotactic insertion on *RR*-LA corresponding to TS2 and TS1 respectively, and (C) isotactic and (D) heterotactic insertion on *SS*-LA, both corresponding to TS1. H atoms omitted for clarity.

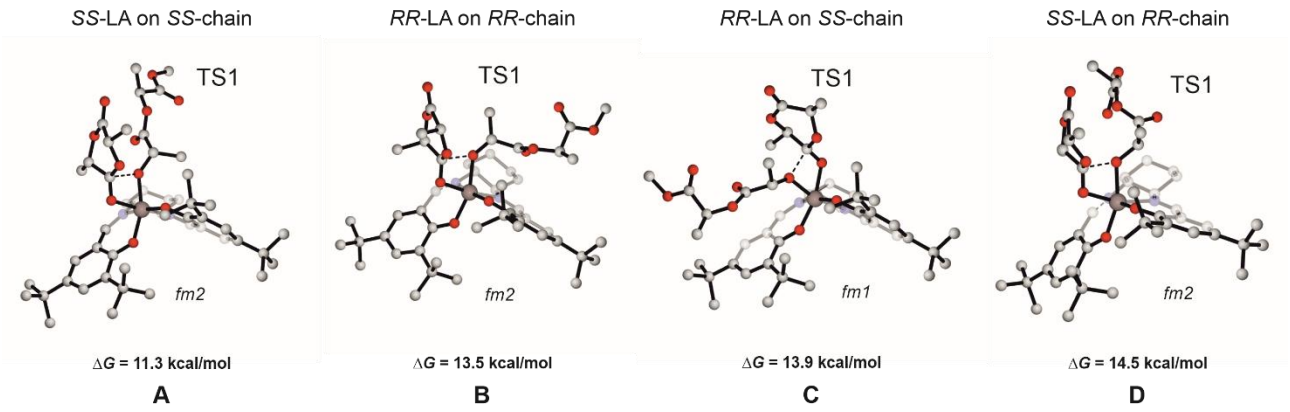

Figure S5. TSs geometries for the RLS of the (*R,R*)-**2A** of (A) isotactic and (B) insertion of respective *RR*-LA and *SS*-LA corresponding both to TS1, and heterotactic insertion on *SS*-LA (C) and *RR*-LA (D), both corresponding to TS1. H atoms omitted for clarity.

Supplementary references

S1 G. W. T. M. J. Frisch, H. B. Schlegel, G. E. Scuseria, M. A. Robb, J. R. Cheeseman, G. Scalmani, V. Barone, G. A. Petersson, H. Nakatsuji, X. Li, M. Caricato, A. Marenich, J. Bloino, B. G. Janesko, R. Gomperts, B. Mennucci, H. P. Hratchian, J. V. Ortiz, A. F. Izmaylov, J. L. Sonnenberg, D. Williams-Young, F. Ding, F. Lipparini, F. Egidi, J. Goings, B. Peng, A. Petrone, T. Henderson, D. Ranasinghe, V. G. Zakrzewski, J. Gao, N. Rega, G. Zheng, W. Liang, M. Hada, M. Ehara, K. Toyota, R. Fukuda, J. Hasegawa, M. Ishida, T. Nakajima, Y. Honda, O. Kitao, H. Nakai, T. Vreven, K. Throssell, J. A. Montgomery, Jr., J. E. Peralta, F. Ogliaro, M. Bearpark, J. J. Heyd, E. Brothers, K. N. Kudin, V. N. Staroverov, T. Keith, R. Kobayashi, J. Normand, K. Raghavachari, A. Rendell, J. C. Burant, S. S. Iyengar, J. Tomasi, M. Cossi, J. M. Millam, M. Klene, C. Adamo, R. Cammi, J. W. Ochterski, R. L. Martin, K. Morokuma, O. Farkas, J. B. Foresman, and D. J. Fox, Wallingford, CT, 2016.

S2 (a) A. D. Becke, *J. Chem. Phys.*, 1993, **98**, 5648-5652; (b) C. Lee, W. Yang and R. G. Parr, *Phys. Rev. B*, 1988, **37**, 785-789.

S3 A. Schäfer, H. Horn and R. Ahlrichs, *J. Chem. Phys.*, 1992, **97**, 2571-2577.

S4 A. D. McLean and G. S. Chandler, *J. Chem. Phys.*, 1980, **72**, 5639-5648.

S5 V. Barone and M. Cossi, *J. Phys. Chem. A*, 1998, **102**, 1995-2001.

S6 (a) S. Grimme, J. Antony, S. Ehrlich and H. Krieg, *J. Chem. Phys.*, 2010, **132**, 154104; (b) S. Grimme, *J. Comput. Chem.*, 2004, **12**, 1463-1473.

S7 N. Spassky, M. Wisniewski, C. Pluta and A. Le Borgne, *Macromol. Chem. Phys.*, 1996, **197**, 2627-2637.

S8 Z. Zhong, P. J. Dijkstra and J. Feijen, *J. Am. Chem. Soc.*, 2003, **125**, 11291-11298.

S9 L. Falivene, Z. Cao, A. Petta, L. Serra, A. Poater, R. Oliva, V. Scarano and L. Cavallo, *Nat. Chem.*, 2019, **11**, 872-879.